The Meteoritical Society

Meteoritics & Planetary Science 48, Nr 5, 796–805 (2013)
doi: 10.1111/maps.12106

Natural occurrence of reidite in the Xiuyan crater of China

Ming CHEN[1*], Feng YIN[2,3], Xiaodong LI[4], Xiande XIE[2], Wansheng XIAO[2], and Dayong TAN[2]

[1]State Key Laboratory of Isotope Geochemistry, Guangzhou Institute of Geochemistry, Chinese Academy of Sciences, Kehua Street 511, Tianhe, Guangzhou 510640, China
[2]Key Laboratory of Mineralogy and Metallogeny, Guangzhou Institute of Geochemistry, Chinese Academy of Sciences, Kehua Street 511, Tianhe, Guangzhou 510640, China
[3]College of Earth Sciences, University of Chinese Academy of Sciences, Beijing 100049, China
[4]Institute of High Energy Physics, Chinese Academy of Sciences, Beijing 100049, China
[*]Corresponding author. E-mail: mchen@gig.ac.cn

(Received 08 January 2013; revision accepted 19 February 2013)

Abstract–The high-pressure minerals of reidite and coesite have been identified in the moderately shock-metamorphosed gneiss (shock stage II, 35–45 GPa) and the strongly shock-metamorphosed gneiss (shock stage III, 45–55 GPa), respectively, from the polymict breccias of the Xiuyan crater, a simple impact structure 1.8 km in diameter in China. Reidite in the shock stage II gneiss displays lamellar textures developed in parental grains of zircon. The phase transformation of zircon to reidite likely corresponds to a martensitic mechanism. No coesite is found in the reidite-bearing gneiss. The shock stage III gneiss contains abundant coesite, but no reidite is identified in the rock. Coesite occurs as acicular, dendritic, and spherulitic crystals characteristic of crystallization from shock-produced silica melt. Zircon in the rock is mostly recrystallized. The postshock temperature in the shock stage III gneiss is too high for the preservation of reidite, whereas reidite survives in the shock stage II gneiss because of relatively low postshock temperature. Reidite does not occur together with coesite because of difference in shock-induced temperature between the shock stage II gneiss and the shock stage III gneiss.

INTRODUCTION

Zircon is a common accessory mineral in igneous, metamorphic, and sedimentary rocks. Reidite is a high-pressure polymorph of zircon ($ZrSiO_4$) with the scheelite-type structure and is about 10% more dense than zircon. Shock-loading experiments reveal that the transition of zircon to reidite takes place at pressure from 30 GPa (Kusaba et al. 1985) to 80 GPa (Gucsik et al. 2004). Reidite can be recovered from shock-loading experiment. Because of a wide distribution of zircon in terrestrial rocks, natural occurrence of reidite has potential importance in identification of shock-metamorphosed rocks and impact sites.

Natural occurrences of reidite have previously been reported from two complex terrestrial impact craters. Reidite was first found in the distal ejecta probably derived from the Chesapeake Bay structure (Glass and Liu 2001; Glass et al. 2002). Subsequently, reidite was identified in the suevite of the Ries crater (Gucsik et al. 2004; Wittmann et al. 2006), and also in the polymict breccia within the Chesapeake Bay structure (Malone et al. 2010).

Coesite has been identified in many terrestrial impact craters, and is an important high-pressure phase for estimation of pressure and temperature conditions of shock metamorphism. The Xiuyan crater is a simple crater in China (Chen et al. 2010, 2011). Abundant coesite has been found in the polymict breccias (Chen et al. 2010a). Here, we report the shock-induced phase transition of zircon to reidite in the shock-metamorphosed rocks from the crater. Our investigation indicates that the occurrence of reidite is distinct from coesite in our samples.

SAMPLES

The Xiuyan crater is a bowl-shaped structure, 1.8 km in diameter. The impact origin of the crater had been documented according to its geological structure

and the shock-metamorphic features of rocks and minerals (Chen et al. 2010, 2011). It is a relatively young crater that formed 50 kyr ago (Chen et al. 2010a; Liu et al. 2013). The crystalline basement rocks of the crater are composed of gneiss-amphibolite-granulites-marble complexes formed in the early Proterozoic Era as well as Jurassic basalt.

The geological drilling at the crater center shows that the crater is filled by Quaternary lacustrine sediments and impact breccias (Fig. 1). The breccias unit 188 m thick is underlain by lacustrine sediments 107 m thick.

The impact breccias in the depth interval from 107 to 260 m are mainly made up of loosely accumulated fragments of rocks up to 30 cm in size. The fragments of rocks are mainly composed of granulite, hornblendite, gneiss, marble, and basalt. Small amount of the polymict breccia were recovered from drill cores in this interval. Most polymict breccias occur in the depth interval from 260 to 295 m, in addition to unconsolidated fragments of rocks. Below the interval from 295 to 307 m is fractured bedrock. The polymict breccias are composed of fragments of gneiss, amphibolites, granulites, marble, basalt, silicate glasses, and fine-grained matrix (Fig. 2). Most loosely accumulated fragments of rocks through the breccias unit are weakly or even not shock-metamorphosed, whereas the polymict breccias contain rock fragments by varying degree of shock metamorphism.

The samples of this investigation are from the polymict breccias recovered from drill cores in the depth interval of 260–295 m. Two types of fragments of shock-metamorphosed gneisses, i.e., the shock stage II gneiss and the shock stage III gneiss, were selected from the polymict breccias for this investigation. A total of 20 thin sections were prepared for this investigation, in which half of them are from the strongly shock-metamorphosed gneiss (shock stage III), and another half from the moderately shock-metamorphosed gneiss (shock stage II). All observations and analyses were performed in situ on the thin sections.

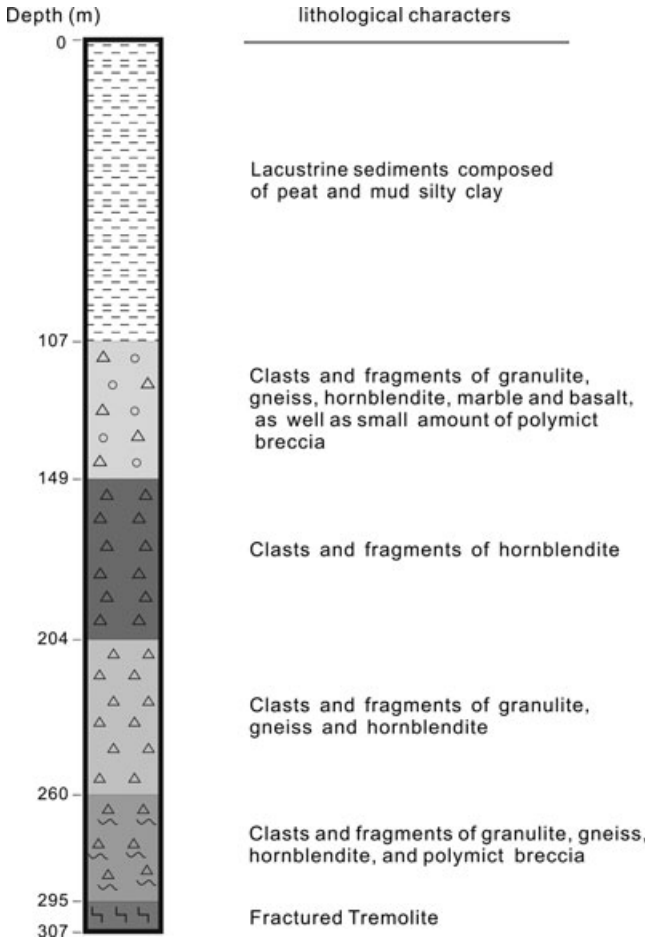

Fig. 1. Schematic stratigraphy of the borehole drilled at the center of the Xiuyan crater.

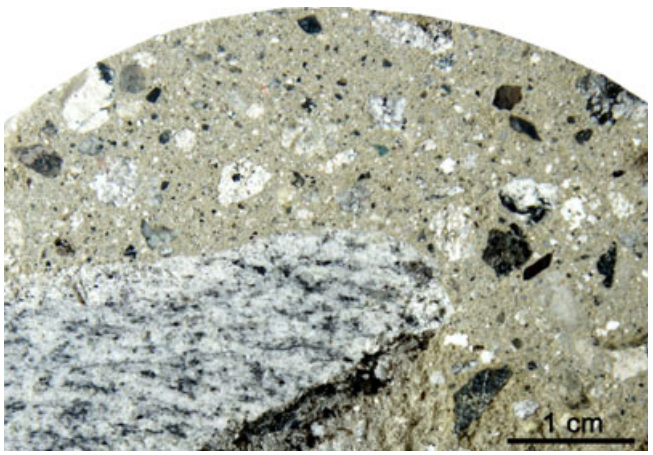

Fig. 2. Polymict breccia from the drill core. There is a big fragment of gneiss at the lower left of the picture.

ANALYTICAL METHODS

Transmitted and reflected light microscopy was used to characterize shock-metamorphic features of rocks and minerals. Raman spectra of minerals were measured by using a Renishaw RM-2000 instrument. A microscope was used to focus the excitation beam (Ar^+ laser, 514 nm line). The size of the laser beam is 1 μm in diameter. Chemical compositions of minerals were determined using a JEOL JXA-8100 electron microprobe at 15 kV accelerating voltage and 10 nA beam current.

In situ micro X-ray diffraction analyses were performed on the thin sections at the 4W2 High Pressure Station of the Beijing Synchrotron Radiation

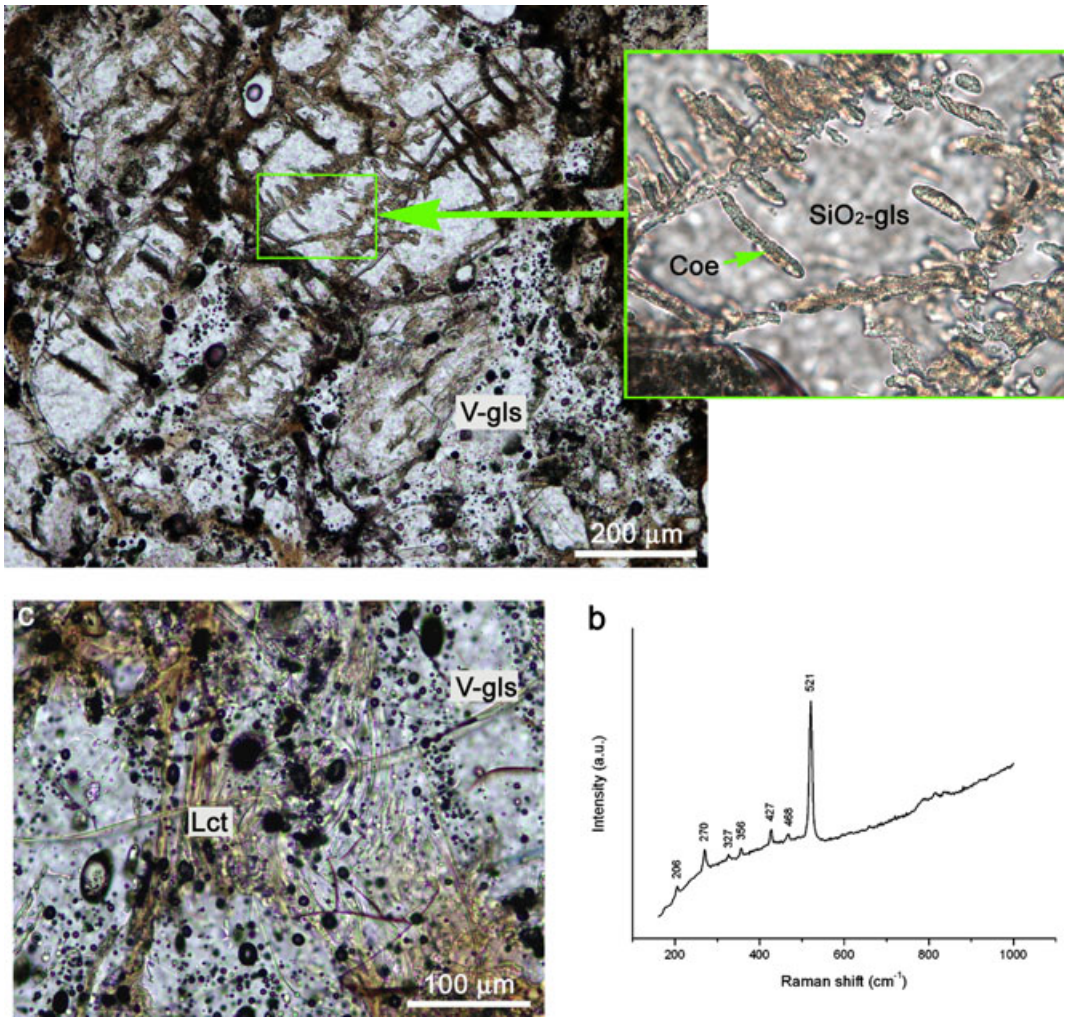

Fig. 3. Optical microscopic images of the shock stage III gneiss in plane-polarized transmitted light. a) Acicular or needle-shaped coesite (Coe) occurring in silica glass (SiO_2-gls). V-gls, vesicular feldspar glass. b) Raman spectrum of coesite displays the peaks at 206, 270, 327, 356, 427, 468, and 521 cm^{-1}. The broad band from 200 to 550 cm^{-1} is attributed to silica glass. c) Lechatelierite with flow texture occurring in vesicular feldspar glass.

Facility with monochromatic X-ray beam $\lambda = 0.6199$Å (calibrated by a CeO_2 standard). The X-rays were focused to 30 (vertical) × 45 (horizontal) μm^2 and the diffraction, collected on a MAR-345 imaging plate, was converted to one-dimensional diffraction profile using the FIT2D software.

RESULTS

Gneiss in the Xiuyan crater consists of quartz (approximately 35%); feldspar (approximately 55%); and hornblende (approximately 10%) and accessory minerals of magnetite, zircon, rutile, and monazite. The shock-metamorphosed gneisses exhibit obvious deformation and phase transformation features in minerals.

The Shock Stage III Gneiss

In the gneiss, feldspars had been completely transformed to vesicular glass (Fig. 3). Amphibole decomposed to oxides mixed with feldspar melt. Two types of silica glasses, mostly coesite-bearing silica glass and a small amount of lechatelierite have been identified. The coesite-bearing silica glass and lechatelierite are enclosed in vesicular feldspar glass.

Coesite-bearing silica glasses usually occur as irregular fragments from several micrometers to several hundred micrometers in size. Most of these grains of silica glass contain coesite. The portion of silica glass is smooth in texture. Coesite commonly occurs as acicular or needle-shaped, dendritic, and spherulitic crystals (Fig. 3a). The acicular or needle-shaped coesite

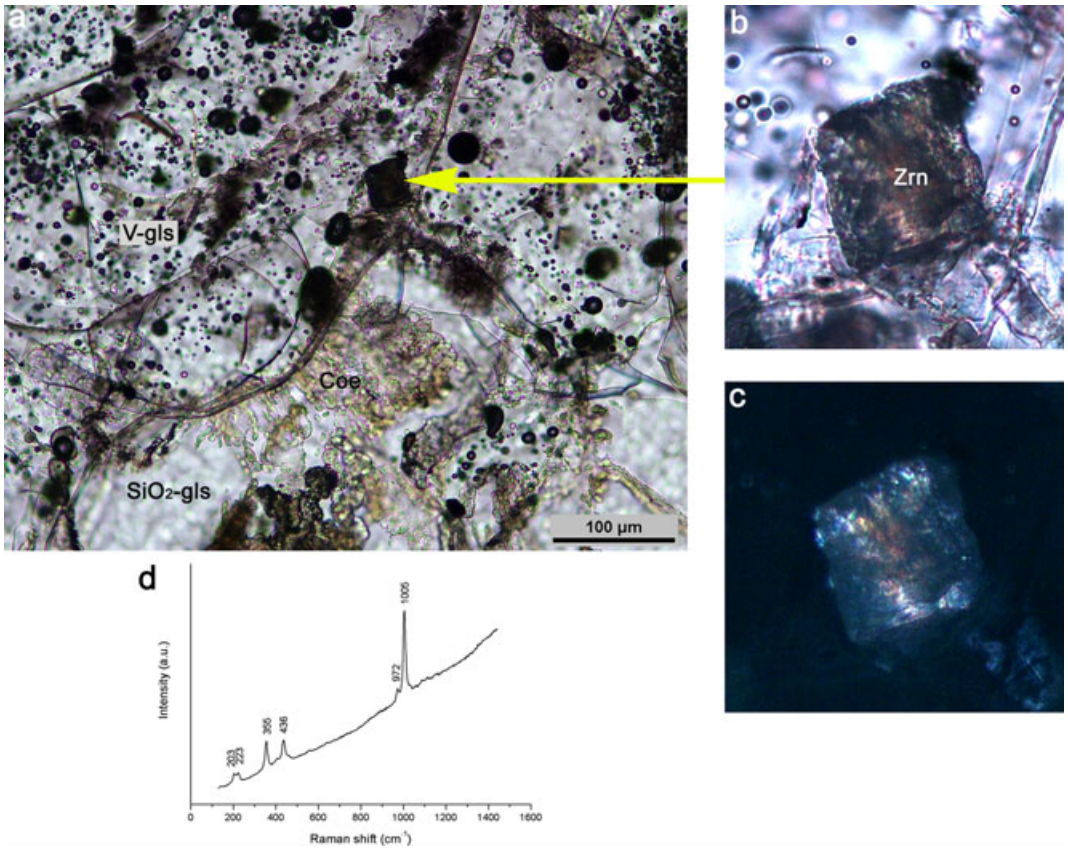

Fig. 4. A zircon (Zrn) on thin section of a shock stage III gneiss sample. a) A zircon associated with the coesite-bearing silica glass (SiO_2-gls) and the vesicular feldspar glass (V-gls), in plane-polarized transmitted light. b) A plane-polarized transmitted light image showing strong deformation of the zircon. c) A cross-polarized transmitted light image of the zircon showing mosaic texture characteristic of polycrystalline aggregates with reduced interference color. d) Raman spectrum of the zircon.

crystals are up to 50 μm in length and 8 μm in width. Some grains of silica glass contain up to 60% coesite. Raman spectrum of coesite displays the peaks at 206(w), 270(m), 327(w), 356(w), 427(m), 468(w), and 521(vs) cm^{-1} (vs, very strong; m, medium; w, weak).

Lechatelierite displays flow textures (Fig. 3b). Some lechatelierites occur in surrounding coesite-bearing glass, but no coesite is observed within lechatelierite.

We investigated about 20 grains of zircon on the thin sections. These grains of zircons are enclosed in vesicular feldspar glass. Some zircons display as idiomorphic crystals (Figs. 4a–c), whereas others occur as irregular clasts. Grain sizes of zircon are from 10 to 100 μm across. Most of the zircon was strongly deformed or fractured. Under transmitted light, zircon commonly exhibits mosaic textures of polycrystalline aggregates with reduced interference color. Grain size of zircon crystallites in polycrystalline aggregates are less than a few micrometers. Raman spectroscopic analysis displays a typical spectrum of zircon with well-defined peaks at 203(w), 223(w), 355(m), 436(m), 972(w), and 1005(s) cm^{-1} (s, strong; m, medium; w, weak) (Fig. 4d). Phase transformation from zircon to reidite as well as phase decomposition of zircon was not observed.

The Shock Stage II Gneiss

In the gneiss, feldspar was strongly deformed and partially transformed to diaplectic glass (Fig. 5). A few feldspar melt pockets up to 200 μm across were observed. Quartz was mostly transformed into an isotropic diaplectic glass showing pseudomorph after quartz (Fig. 6). At high magnification, some traces of multiple sets of PDFs can be observed in the diaplectic quartz glass (Fig. 6c). Hornblende was partially decomposed into iron-magnesium oxides. No coesite was found in the sample.

About 30 grains of zircon in the gneiss were investigated on the thin sections. Grain sizes of zircon are from 20 to 150 μm across. Most of the zircon crystals were strongly deformed and fractured (Figs. 7

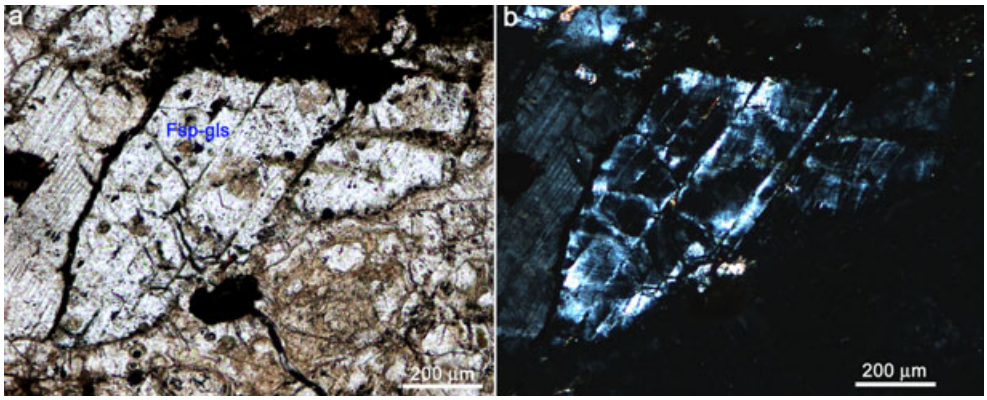

Fig. 5. Optical microscopic images of diaplectic feldspar glasses in the shock stage II gneiss. a) Diaplectic feldspar glass (Fsp-gls) with original morphology, in plane-polarized transmitted light. b) A cross-polarized transmitted light image of the feldspar grain in (a) showing partial transformation to isotropic diaplectic glass (Fsp-gls) with some residues of feldspar.

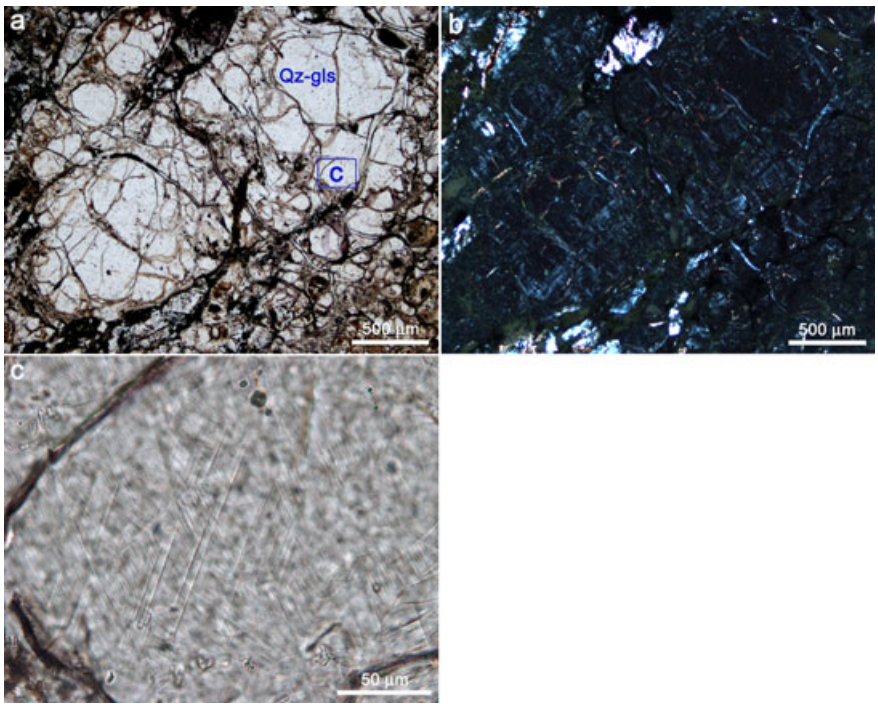

Fig. 6. Optical microscopic images of diaplectic quartz glasses in the shock stage II gneiss. a) Diaplectic quartz glass (Qz-gls) with original shape of grains, in plane-polarized transmitted light. b) A cross-polarized transmitted light image of the quartz in (c) showing optical extinction of diaplectic quartz glass (Qz-gls). c) High-magnification image of diaplectic quartz glass in (a) showing some traces of multiple sets of PDFs.

and 8). The zircon crystals commonly display very low interference colors or locally become isotropic. Lamellar textures were observed in the zircon crystal. Figure 7a displays a zircon intersected by multiple sets of lamellae less than 1 μm in thickness. Thin layers up to 5 μm, which are aggregates of lamellae, are also observed (Fig. 8).

In situ Raman spectroscopic analyses were conducted at the lamellae in zircons (Fig. 9). In addition to the Raman peaks from zircon, other peaks at 300(w), 330(w), 407(s), 462(s), 560(s), 611(w), 846(s), and 885(s) cm^{-1} (s, strong; w, weak) can be attributed to the scheelite-type $ZrSiO_4$ (Knittle and Williams 1993; Gucsik et al. 2004b). The natural scheelite-type $ZrSiO_4$ is reidite, a high-pressure polymorph of zircon (Glass et al. 2002). Among 30 investigated zircon grains, reidite was found in seven grains. These reidite-zircon grains contain 5 to 30% reidite.

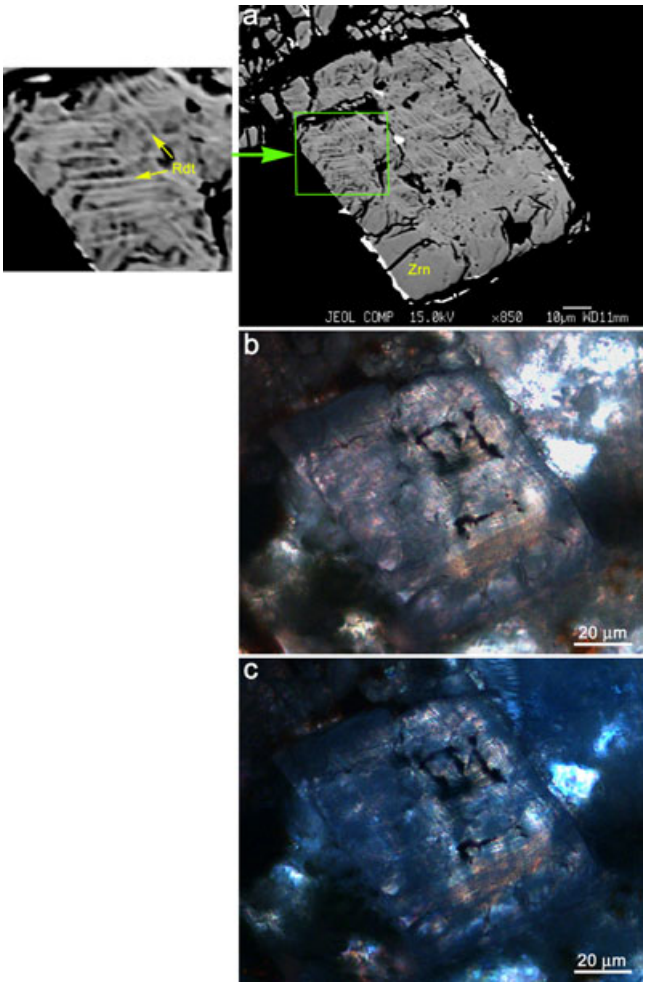

Fig. 7. A zircon (Zrn) partially transformed to reidite (Rdt) in the shock stage II gneiss. a) A backscattered electron image of lamellar textures in this zircon-reidite grain shows that the zircon is intersected by two sets of lamellar reidite less than 1 μm in thickness. b) A plane-polarized transmitted light image of the zircon in (a) showing strong deformation of the zircon. c) A cross-polarized transmitted light image of the zircon in (b) showing low interference color and local isotropy.

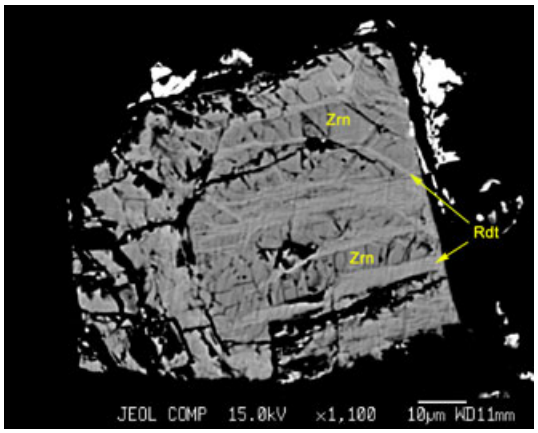

Fig. 8. A backscattered electron image showing a strongly deformed reidite-bearing zircon in the shock stage II gneiss. Thin layers of reidite (Rdt) up to 5 μm are identified in zircon (Zrn). Reidite appears much brighter than zircon in the image due to its higher density.

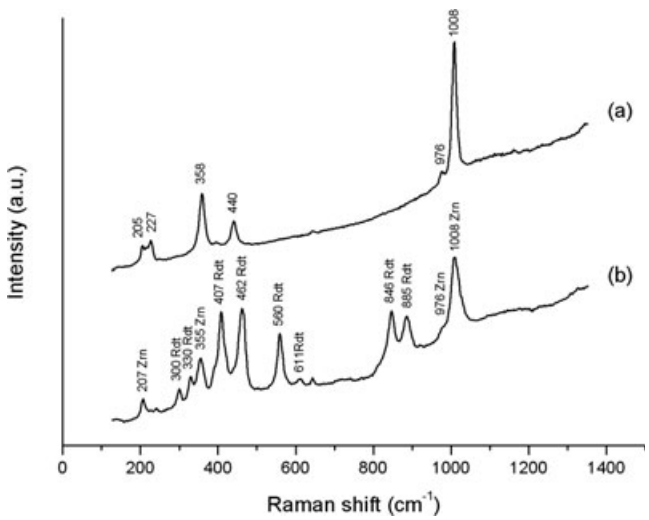

Fig. 9. Raman spectra of a reidite-bearing zircon. a) Raman spectrum of the zircon consists of peaks at 205, 227, 358, 440, 976, and 1008 cm^{-1}; b) Raman spectrum from two phase mixture of reidite (Rdt) and zircon (Zrn). Raman peaks at 300, 330, 407, 462, 560, 611, 846, and 885 cm^{-1} are attributed to reidite.

Micro X-ray diffraction analysis was conducted in situ in the zircon with lamellae of reidite on thin section. At a fixed orientation of sample, we collected arc-like diffraction patterns (Fig. 10). Twenty-one diffraction lines were collected (Table 1). The reflections are mostly indexed to reidite and zircon. In addition, a few weak reflections could be indexed to stishovite and baddeleyite, which provides evidence for a small amount of decomposition of $ZrSiO_4$ to ZrO_2 plus SiO_2. Eleven reflections collected from reidite are in agreement with the synthesized scheelite-type $ZrSiO_4$ (Liu 1979) and the natural reidite (Glass et al. 2002). The lattice parameters are $a = 4.749$ (3) Å, $c = 10.43$ (1) Å, $V = 235.2(3)$ Å^3 with $Z = 4$. The intensities of reflections from both reidite and zircon change along with different orientation of the sample. The zircon was originally a single crystal. The arc-like diffraction lines of zircon show strong deformation and fragmentation of the crystal. The arc-like diffraction lines from reidite could be indicative of preferred orientation of multiple sets of lamellae of reidite. The collected reflections from zircon are much stronger than those from reidite, which

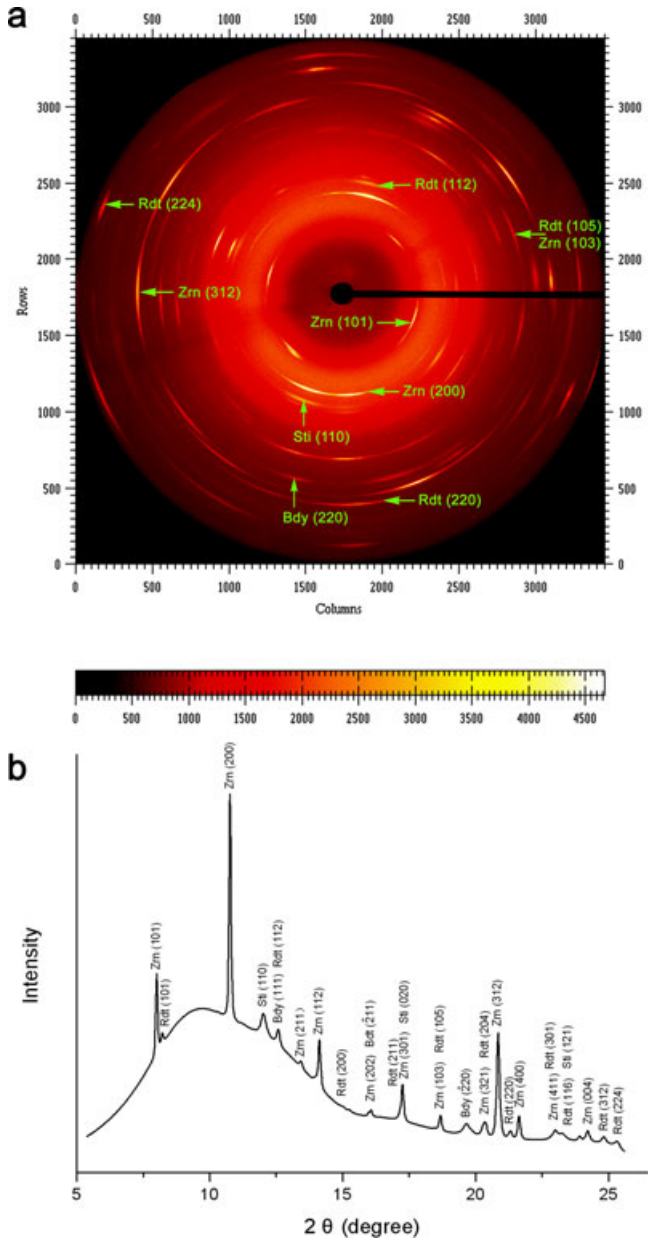

Fig. 10. X-ray diffraction pattern obtained from a zircon with lamellae of reidite from Fig. 7a at a fixed orientation of the sample. a) The X-ray diffraction image shows arc-like diffraction patterns, which can be indexed to zircon (Zrn), reidite (Rdt), stishovite (Sti), and baddeleyite (Bdy). b) Eleven reflections from reidite (Rdt) have been collected in addition to zircon (Zrn), stishovite (Sti), and baddeleyite (Bdy).

indicates that partial zircon was only partially transformed to reidite.

Quantitative analytical results of chemical compositions in zircon and reidite are given in Table 2. The compositions between both minerals are very similar.

Table 1. Indexed peaks of the X-ray diffraction pattern and Miller indices collected for reidite-bearing zircon.

		Reidite		Zircon	Stishovite	Baddeleyite
d_{obs} (Å)	I	hkl	d_{cal} (Å)	hkl	hkl	hkl
4.434	30			101		
4.326	<5	101	4.322			
3.301	100			200		
2.960	20				110	
2.829	10	112	2.829			111
2.651	<5			211		
2.520	20			112		
2.372	<5	200	2.374			
2.218	<5			202		$\bar{2}$ 11
2.078	20	211	2.801	301	020	
1.909	10	105		103		
1.816	10					$\bar{2}$ 20
1.756	10	204	1.755	321		
1.713	40			312		
1.677	<5	220	1.679			
1.652	15			400		
1.564	<5	301	1.565	411		
1.538	<5	116	1.543		121	
1.496	<5			004		
1.441	<5	312	1.443			
1.413	<	224	1.412			

d_{obs} and d_{cal} are observed and calculated d values, respectively.

Table 2. Chemical compositions of zircon and reidite.

	Zircon		Reidite	
	(6)	STDEV	(5)	STDEV
SiO_2	33.50	0.46	33.19	0.43
ZrO_2	64.55	1.52	63.98	1.22
HfO_2	1.35	0.20	1.65	0.18
ThO_2	0.05	0.05	0.09	0.07
TiO_2	0.05	0.03	n.d.	
Al_2O_3	n.d.		n.d.	
Cr_2O_3	0.04	0.03	0.03	0.02
CaO	0.06	0.04	0.07	0.04
FeO	0.19	0.17	0.24	0.13
MgO	n.d.		n.d.	
MnO	n.d.		n.d.	
Totals	99.79		99.25	

All data in weight %. The number in parentheses is the number of analyses (n.d., not detected; STDEV, standard deviation).

DISCUSSION

Shock Stages

The Xiuyan crater is a simple crater, in which the shock-produced phase transition of zircon to reidite has been identified. The occurrence of reidite in terrestrial

impact craters was shown to occur mainly in shock stage II–III that experienced shock pressures of 35–50 GPa and postshock temperatures of 300–1100 °C (Gucsik et al. 2004; Wittmann et al. 2006).

In the shock stage II gneiss from the Xiuyan crater, nearly all quartz is transformed to diaplectic glass, and feldspars are partially transformed to diaplectic glass. Diaplectic glass is a glass formed by solid-state transformation of mineral without melting (Chao 1967; Engelhardt et al. 1967; Stöffler and Langenhorst 1994; Grieve et al. 1996). The existence of traces of PDFs in the diaplectic quartz glass shows that the glass does not experience shock-melting. The PDFs in quartz should have been produced during the shock compression, and some traces of PDFs were preserved although whole grains of quartz later became amorphized. It is well established that quartz transforms to diaplectic glass at pressure from 35 to 50 GPa, and starts to melt at pressures above 50 GPa (Stöffler and Langenhorst 1994; Grieve et al. 1996). Feldspar transforms to displectic glass at pressure from 30 to 43 GPa, and melts at pressure above 43 GPa (Stöffler 1972; Harrison and Hörz 1981; Velde et al. 1989; French 1998). Since most of quartz and feldspar were transformed to diaplectic glasses, the shock stage II gneiss in the Xiuyan crater experienced shock pressures of 35–45 GPa (Stöffler 1971; Metzler et al. 1988; Grieve et al. 1996), which corresponds to the postshock temperature of 300–900 °C (Grieve et al. 1996). The existence of a few melt pockets are unlikely to be related to the equilibrium shock pressure and temperature experienced by the whole rock, and should be attributed to localized spikes of pressure and temperature that occur in shock-metamorphosed polycrystalline rocks (Stöffler et al. 1991; Schmitt 2000).

In the shock stage III gneiss, quartz was mostly transformed into silica glass and partially into lechatelierite, a fused silica glass. Coesite occurs in the silica glass with the shapes of fragments. Feldspars were completely melted and became vesicular glass. Based on the classification of shock stages in nonporous quartz-feldspathic rocks (Stöffler and Grieve 2007), the shock stage III gneiss experienced shock pressures of 45–55 GPa (Stöffler 1971; Metzler et al. 1988; Grieve et al. 1996). Although the silica glass occurs as the shapes of irregular fragments, the silica glass had been melting. The silica glass is smooth in texture. Distinct from the diaplectic quartz glass in the shock stage II gneiss, no trace of PDFs can be observed in the silica glass. It shows that any possible deformation feature including PDFs, which is caused by compression, will be erased because of subsequent melting. The morphologies of acicular or needle-shaped, dendritic, and spherulitic aggregates of coesite enclosed in the silica glass indicate that coesite crystallizes from silica melt in the P-T stability field of coesite. Postshock temperature increases during decompression. Thus, coesite should have crystallized during decompression with elevated temperature. It is well accepted that the formation of lechatelierite in the crystalline rocks requires a peak shock pressure >50 GPa (Stöffler and Langenhorst 1994; Grieve et al. 1996). At ambient pressure, the melting temperature of quartz is around 1500 °C (Zhang et al. 1996). Therefore, the peak postshock temperature in the shock stage III gneiss is estimated to be above 1500 °C.

Shock-Induced Transition of Zircon to Reidite

Shock-induced transition of zircon to reidite is experimentally achieved at pressures from 30 to 80 GPa (Mashimo et al. 1983; Kusaba et al. 1985; Leroux et al. 1999; Gucsik et al. 2004b). In comparison to the pressure of shock-loading experiments, the peak shock pressure of 35–45 GPa in the shock stage II gneiss of the Xiuyan crater should have resulted in the transition of zircon to reidite. Reidite reverts rapidly to zircon when heated to 1200 °C at ambient pressure (Kusaba et al. 1985). The average shock temperature in the shock stage II gneiss (<900 °C) allows the preservation of shock-produced reidite. The existence of a few melt pockets in the gneiss shows a local deviation of temperature from average value. Reidite decomposes to ZrO_2 plus SiO_2 above 22 GPa at about 1000 °C (Liu 1979). Trace amounts of stishovite and baddeleyite in the reidite-bearing zircon could indicate that the shock temperature in the rock is generally too low for extensive decomposition of reidite.

A martensitic phase transformation mechanism, which involves no long-range diffusion of atoms, was proposed to explain shock-induced phase transition of zircon to reidite under shock compression (Kusaba et al. 1986; Leroux et al. 1999). It was suggested that the [110] direction of zircon is converted by simple shearing to the [001] direction of reidite (Kusaba et al. 1986), or that the crystallographic relationships between zircon and reidite are $\{100\}_z$ //$\{112\}_s$ and $[001]_z$ // $<110>_s$ (Leroux et al. 1999). Natural reidite from the distal ejecta probably derived from the Chesapeake Bay structure shows clear lamellar textures, and the formation of the lamellae was attributed to a martensitic transformation mechanism (Glass and Liu 2001; Glass et al. 2002). The lamellar textures of reidite in the Xiuyan crater is consistent with the features reported by Glass and Liu (2001) and Glass et al. (2002), hence supporting a martensitic mechanism. The arc-like X-ray diffraction patterns of reidite and zircon in our samples show the deformation of crystals on one

hand and on the other hand some preferred orientations of reidite that occur along certain crystallographic orientations of zircon, which support a lamellar texture.

Shock-Induced Recrystallization of Zircon

For the shock stage III gneiss of the Xiuyan crater, a peak shock pressure about 50 GPa is within the pressure range (30–80 GPa) for shock-induced transition of zircon to reidite. However, we observe no reidite, but coesite is abundant in the gneiss. The coesite forms by crystallization from silica melt during decompression with elevated shock temperature. The existence of lechatelierite in the rock shows a peak postshock temperature above 1500 °C. Reidite will revert rapidly to zircon above 1200 °C after pressure release (Kusaba et al. 1985). If the transition of zircon to reidite did take place under compression, reidite would not survive subsequent high temperature resulting in melting of quartz. At such high temperature, coesite can be preserved because it is a superheated crystal that is stable up to 1500 °C at room pressure (Bourova et al. 2006).

Under shock-produced high temperature, strongly deformed zircons in the shock stage III gneiss, which are mostly enclosed in vesicular feldspar melt, were recrystallized. As we have seen, most zircons display mosaic textures characteristic of polycrystalline aggregates.

CONCLUSIONS

Impact-produced polymict breccias from the Xiuyan crater contain rock fragments by varying degree of shock metamorphism, in which reidite and coesite have been identified in the moderately shock-metamorphosed gneiss and strongly shock-metamorphosed gneiss, respectively. The moderately shock-metamorphosed gneiss corresponds to the shock stage II (35–45 GPa). Reidite was produced in the rock and occurs as multiple sets of lamellae in zircon. The phase transformation of zircon to reidite took place during compression likely via a martensitic mechanism. No coesite is found in the rocks. The strongly shock-metamorphosed gneiss corresponds to the shock stage III (45–55 GPa). Abundant coesite was produced in the rock, where coesite was crystallizing from silica melt during decompression with elevated temperature. Zircon in the rock was recrystallized and commonly occurs as polycrystalline aggregates. No reidite is found in the rock. The postshock temperature in the shock stage III gneiss is too high for the preservation of reidite, whereas reidite survives in the shock stage II gneiss because of relatively low postshock temperature.

Acknowledgments—We are grateful to C. Koeberl, A. Wittman, and an anonymous reviewer for constructive comments and suggestions on our manuscript. This work was supported by NNSF of China (Grant No. 41172044) and GIG CAS 135 Project (Grant No. Y234071001). This is contribution No. IS-1627 from GIGCAS.

Editorial Handling—Dr. Christian Koeberl

REFERENCES

Bourova E., Richet P., and Petitet J. P. 2006. Coesite (SiO_2) as an extreme case of superheated crystal: An X-ray diffraction study up to 1776 K. *Chemical Geology* 229:57–63.

Chao E. C. T. 1967. Shock effects in certain rock-forming minerals. *Science* 156:192–202.

Chen M., Xiao W., Xie X., Tan D., and Cao Y. 2010a. Xiuyan crater, China: Impact origin confirmed. *Chinese Science Bulletin* 55:1777–1781.

Chen M., Xiao W., and Xie X. 2010b. Coesite and quartz characteristic of crystallization from shock-produced silica melt in the Xiuyan crater. *Earth and Planetary Science Letters* 297:306–314.

Chen M., Koeberl C., Xiao W., Xie X., and Tan D. 2011. Planar deformation features in quartz from impact-produced polymict breccia of the Xiuyan crater, China. *Meteoritics & Planetary Science* 46:729–736.

Engelhardt W. von, Arndt J., Stöffler D., Müller E. F., Jeziprkowski H., and Gubser R. A. 1967. Diaplectische Gläser in den Breccien des Ries von Nördlingen als Anzeichen für Stoßwellenmetamorphose. *Contributions to Mineralogy and Petrology* 15:91–100.

French B. M. 1998. *Traces of catastrophe: A handbook of shock-metamorphic effects in terrestrial meteorite impact structures*. LPI Contribution 954. Houston, Texas: Lunar and Planetary Institute. 120 p.

Glass B. P. and Liu S. 2001. Discovery of high-pressure $ZrSiO_4$ polymorph in naturally occurring shock-metamorphosed zircons. *Geology* 29:371–373.

Glass B. P., Liu S., and Leavens P. B. 2002. Reidite: An impact-produced high-pressure polymorph of zircon found in marine sediments. *American Mineralogist* 87:562–565.

Grieve R. A. F., Langenhorst F., and Stöffler D. 1996. Shock metamorphism of quartz in nature and experiment: II. Significance in geoscience. *Meteoritics & Planetary Science* 31:6–35.

Gucsik A., Koeberl C., Brandstätter F., Libowitzky E., and Reimold W. U. 2004a. Cathodoluminescence, electron microscopy, and Raman spectroscopy of experimentally shock metamorphosed zircon crystals and naturally shocked zircon from the Ries impact crater. In *Cratering in marine environments and on ice*, edited by Dypvik H., Burchell M., and Claeys P. Heidelberg, Germany: Springer-Verlag. pp. 281–322.

Gucsik A., Zhang M., Koeberl C., Salje E. K. H., Redfern S. A. T., and Pruneda J. M. 2004b. Infrared and Raman spectra of $ZrSiO_4$ experimentally shocked at high pressures. *Mineralogical Magazine* 68:801–811.

Harrison W. J. and Hörz F. 1981. Experimental shock metamorphism of calcic plagioclase. Proceedings, 12th Lunar and Planetary Science Conference. pp. 395–397.

Knittle E. and Williams Q. 1993. High-pressure Raman spectroscopy of $ZrSiO_4$: Observation of the zircon to scheelite transition at 300 K. *American Mineralogist* 78:245–252.

Kusaba K., Syono Y., Kikuchi M., and Fukuoka K. 1985. Shock behavior of zircon: Phase transition to scheelite structure and decomposition. *Earth and Planetary Science Letters* 72:433–439.

Kusaba K., Yagi T., Kikuchi M., and Syono Y. 1986. Structural considerations on the mechanism of the shock-induced zircon–scheelite transition in $ZrSiO_4$. *Journal of Physics and Chemistry of Solids* 47:675–679.

Leroux H., Reimold W. U., Koeberl C., Hornemann U., and Doukhan J. C. 1999. Experimental shock deformation in zircon: A transmission electron microscopic study. *Earth and Planetary Science Letters* 169:291–301.

Liu L. G. 1979. High-pressure phase transformations in baddeleyite and zircon, with geophysical implications. *Earth and Planetary Science Letters* 44:390–396.

Liu K. X., Chen M., Ding X. F., Fu D. P., Ding P., Shen C. D., and Xiao W. S. 2013. AMS radiocarbon dating of lacustrine sediment from an impact crater in northeastern China. *Nuclear Instruments and Methods in Physics Research Section B* 294:593–596.

Malone L., Boonsue S., Spray J., and Wittmann A. 2010. Zircon-reidite relations in breccias from the Chesapeake Bay impact structure (abstract #2286). 41st Lunar and Planetary Science Conference. CD-ROM.

Mashimo T., Nagayama K., and Sawaoka A. 1983. Shock compression of zirconia ZrO_2 and zircon $ZrSiO_4$ in the pressure range up to 150 GPa. *Physics and Chemistry of Minerals* 9:237–247.

Metzler A., Ostertag R., Redeker H. J., and Stöffler D. 1988. Composition of the crystalline basement and shock metamorphism of crystalline and sedimentary target rocks at the Haughton impact crater, Devon Island, Canada. *Meteoritics* 23:197–207.

Schmitt R. T. 2000. Shock experiments with the H6 chondrite Kernouvé: Pressure calibration of microscopic shock effects. *Meteoritics & Planetary Science* 35:545–560.

Stöffler D. 1971. Progressive metamorphism and classification of shocked and brecciated crystalline rocks at impact craters. *Journal of Geophysical Research* 76:5541–5551.

Stöffler D. 1972. Deformation and transformation of rock-forming minerals by natural and experimental shock processes. I. Behavior of minerals under shock compression. *Fortschritte Mineralogie* 49:50–113.

Stöffler D. and Grieve R. A. F. 2007. Impactites. In *Metamorphic rocks: A classification and glossary of terms, recommendations of the International Union of Geological Sciences*, edited by Fettes D. and Desmons J. Cambridge, UK: Cambridge University Press. pp. 82–92, 111–125, and 126–242.

Stöffler D. and Langenhorst F. 1994. Shock metamorphism of quartz in nature and experiment: I. Basic observation and theory. *Meteoritics* 29:155–181.

Stöffler D., Keil K., and Scott E. R. D. 1991. Shock metamorphism of ordinary chondritis. *Geochimica et Cosmochimica Acta* 55:3845–3867.

Velde B., Syono Y., Kikuchi M., and Boyer H. 1989. Raman microprobe study of synthetic diaplectic plagioclase feldspars. *Physics and Chemistry of Minerals* 16:436–441.

Wittmann A., Kenkmann T., Schmitt R. T., and Stöffler D. 2006. Shock-metamorphosed zircon in terrestrial impact craters. *Meteoritics & Planetary Science* 41:433–454.

Zhang J., Li B., Utsmi W., and Liebermann R. C. 1996. In situ X-ray observations of the coesite-stishovite transition: Reversed phase boundary and kinetics. *Physics and Chemistry of Minerals* 23:1–10.